Hindawi
Geofluids
Volume 2021, Article ID 6655431, 12 pages
https://doi.org/10.1155/2021/6655431

*Research Article*

# New View on the Genesis of the Bashuihe Pluton, Laoshan Granites, China: Indications from Fluid Inclusions and H–O Isotopes

**Huimin Liu**,[1] **Zhaojun Song**,[1,2] **Hongbo Yan**,[1,3] **Wenyu Wang**,[1,4] **Xinru Wang**,[1] **Yifang Sun**,[1] **and Haonan Li**[1]

[1]*College of Earth Science and Engineering, Shandong University of Science and Technology, Qingdao 266590, China*
[2]*Laboratory for Marine Geology, Qingdao National Laboratory for Marine Science and Technology, Qingdao 266061, China*
[3]*Jinjie Coal Mine, Shenhua Shendong Coal Group Corporation Limited, Yulin 719319, China*
[4]*Key Laboratory of Marine Geology and Metallogeny, First Institute of Oceanography, Ministry of Natural Resources, Qingdao 266061, China*

Correspondence should be addressed to Zhaojun Song; songzhaojun76@163.com

Received 10 December 2020; Revised 11 January 2021; Accepted 23 January 2021; Published 8 February 2021

Academic Editor: Feng Xiong



Oval caves have recently been discovered in the Bashuihe granite pluton of Laoshan Mountain, China. Oval caves typically occur in alkaline granites. This study conducted microthermometry and stable isotope analysis of quartz inclusions from oval caves and host rocks from the Bashuihe pluton to reconstruct the diagenetic evolutionary history of the Laoshan area. The temperature measurement results indicated a homogenisation temperature range from 162.5 to 261.6°C (mean 203.9°C), a salinity range of 2.1–8.3 wt% (mean 5.07 wt%), and a density range of 0.8–0.98 g/cm$^3$ (mean 0.90 g/cm$^3$), indicating a low-temperature, low-salinity, and low-density fluid. The emplacement depth ranged from 2.73 km to 4.43 km, indicating medium-shallow granite. A hydrogen and oxygen isotope analysis ($\delta D = -83.58 - -67.17$, $\delta^{18}O_{H_2O} = 0.83 - 0.39$) revealed that the diagenetic fluids of the Bashuihe pluton represented a mixed hydrothermal solution composed of meteoric water and magmatic water. The results of a whole rock, H–O isotopes, rare earth element, and high field strength element analysis on the Laoshan alkali granites suggest significant hydrothermal activity in the late stage of magmatism. Primary oval caves in the Bashuihe pluton most likely evolved in the following sequence: fluid was enriched in the late diagenetic stage, diagenetic minerals crystallised under low temperature and pressure conditions, the crystallisation rate accelerated, and the magma condensed rapidly. Moreover, the increase in magma fluid enabled the movement and convergence of fluid. The accumulated fluid and volatiles occupied more space, and rapid magma condensation trapped the accumulated fluid and volatiles in the pluton, forming the oval granite cave. This research provides a crucial theoretical reference for the development and utilisation of underground space and engineering buildings in granite regions.

## 1. Introduction

The granite landforms are complex and diverse [1, 2], because they are in different forming environments and transformation of complex tectonics, climate, and other environmental factors in the later period [3, 4]. It is the result of the interaction of multiple factors of geological internal and external forces. It is also an important part of understanding the critical zone of the earth [2, 5]. Their causes are one of the focuses of international academia. Granites are widely distributed in China [6]. The superior geographical location and unique geological and geomorphological characteristics of the Laoshan area are typical of granite landforms in eastern China [7]. Therefore, these granites are popular research areas for many geologists [5, 8, 9]. Previous studies have established the age [10, 11], geochemical characteristics [12, 13], and magmatic structural background of the Laoshan granite [14, 15].

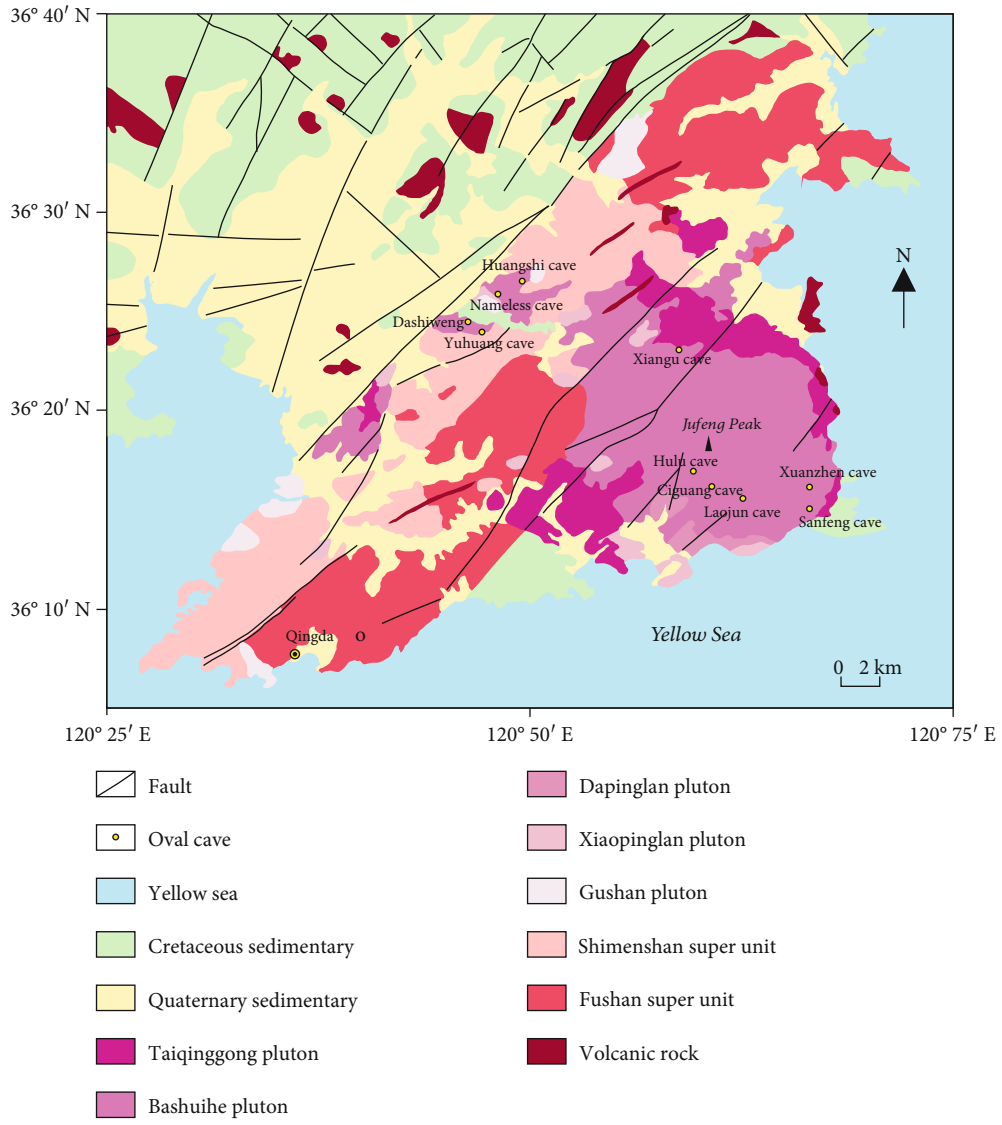


Figure 1: Regional geological map of Laoshan (modified from [30]).

In recent years, the possible glacial origin of the pit-like microtopography of granites in eastern China has become critical in determining glacier development during the Quaternary period in eastern China [16, 17]. The pit-like microtopography on the surface of the Laoshan granite is a possible indicator of glacial origin. However, uncertainty remains about the genesis of pit-like microtopography in the Laoshan area [5, 17, 18]. Previous studies suggested that the miarolitic structure of the Laoshan granite had an important impact on the pit-like microtopography development in the Laoshan area. Most of the pit-like microtopography is developed on the base of a miarolitic cave [5, 19, 20]. Moreover, more than ten large oval caves with a diameter of 1–3 m were found in the Laoshan area. The walls of these caves are relatively smooth, and the overall shape is ellipsoidal. Several caves are famous tourist attractions, such as the Yuhuang and Ciguang caves. However, several caves are remote and inaccessible, such as the Xiangu cave and Huangshi cave. The shape of these oval caves is closely related to the large pit-like microtopography, supporting the theory of a miarolitic structure origin [21]. Song and others suggested that the large pit-like microtopography represents granite primary caves formed directly after joint cutting and exposure or by later transformation [14, 19, 22].

However, the formation and diagenetic environment of the Laoshan pluton with a large oval hole are not apparent. This study conducted fluid inclusion petrographic temperature measurements and stable isotope studies on quartz inclusions from the Laoshan pluton, where the oval caves are located, to determine the characteristic source of its diagenetic fluids. Furthermore, the formation mechanism of the oval caves in the Laoshan granite was analysed to provide a theoretical basis for guiding the further study of bubble cave formation. Unlike the previously known joints, faults, veins, bedding planes, and other cracks, oval holes are not common in crustal rocks. But discontinuities in this naturally occurring rock mass usually contain complex networks and dominate the geomechanics of underground rocks [23–28]. This

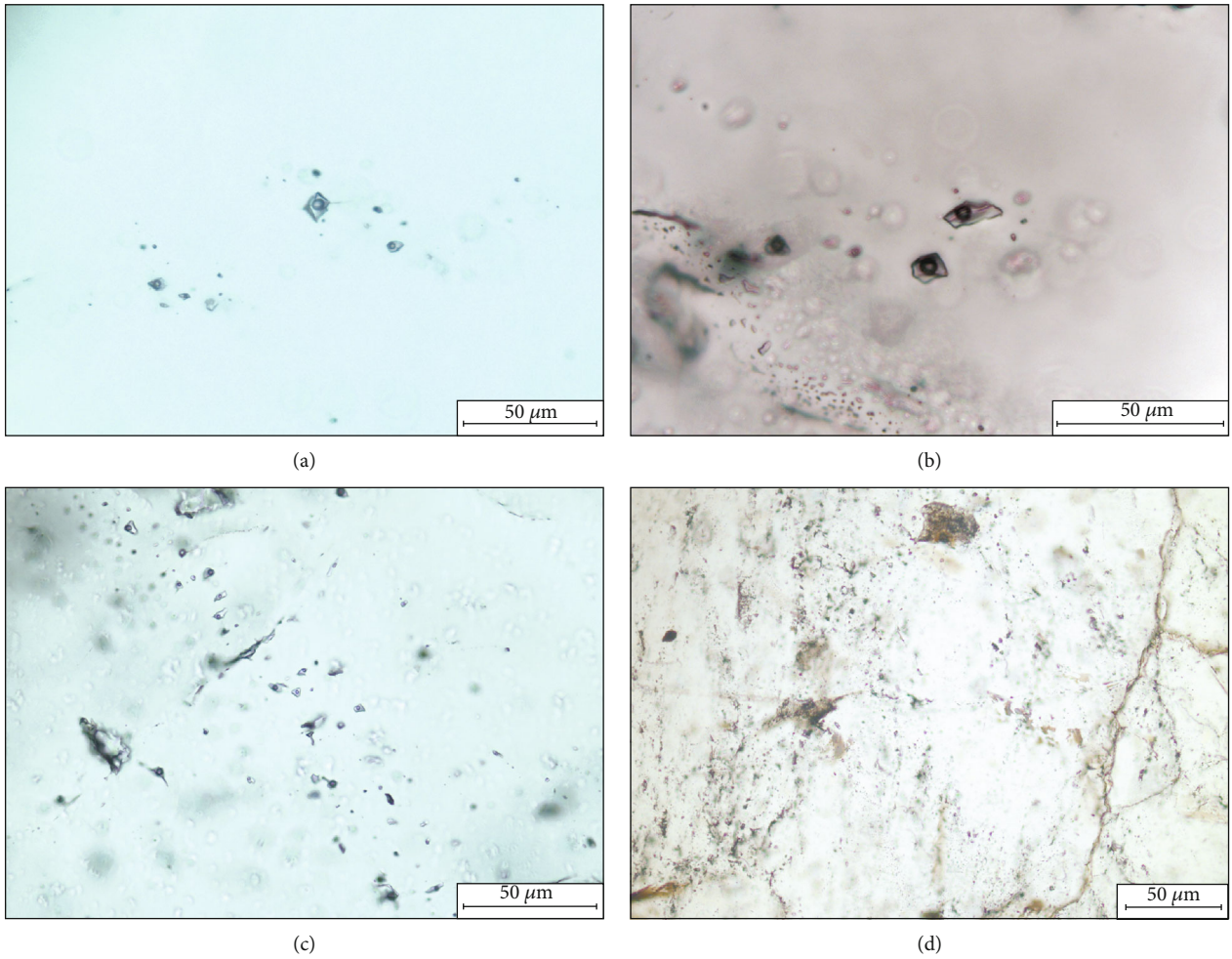


Figure 2: Fluid inclusions distributed in quartz: (a, b) star distribution; (c) strip distribution; (d) predominate group distribution.

research provides a crucial theoretical reference for the development and utilisation of underground space and engineering buildings in granite regions.

## 2. Materials and Methods

*2.1. Geological Background.* Magmatic rocks in the Laoshan area developed from multiple magmatic invasions. Numerous lithologic types with complex structures exist in the area, which were predominately formed in the late Yanshan period. Most of the plutons are distributed in a ring shape. Grain sizes varying from medium-coarse-grained, medium-grained, medium-fine-grained, and fine-grained to fine spots in the granites represent early to late stages of structural evolution. Each pluton exhibits a complete structural evolutionary sequence consistent with homologous magma. According to the composition and structural evolution of the region, Laoshan granite can be divided into three types: (1) Fushan monzogranite, (2) Shimenshan syenite granite, and (3) Laoding alkali feldspar granite [8, 29]. Each type is a sub-super unit, and the distribution of each sub-super unit is shown in Figure 1. The loading sub-super unit is further divided into six plutons: Gushan, Yuhuangshan, Xiaopinglan, Dapinglan, Bashuihe, and Taiqinggong. This study predominately focused on the Bashuihe pluton comprising typical A-type granite, also called miarolitic granite, because of its well-developed miarolitic structure. This type of granite is mainly formed in an environment where the crust transitions from compression to tension. Moreover, previous studies have determined that the Bashuihe pluton formed under the conditions of shallow magmatic emplacement depth, low pressure, and rapid cooling rate. The rapid condensation rate of magma during pluton formation resulted in the entrapment of volatile bubbles in pluton and formation of small caves. Later, some of the caves were affected by hydrothermal activity and developed crystals, forming the characteristic miarolitic structure visible today. The granites in the study area are predominately medium-coarse-grained alkaline granites. The zircon U-Pb age is 114.2 Ma, $SiO_2$ content is between 72% and 77%, $K_2O + Na_2O$ content ranges from 8.6 to 9.1%, $Al_2O_3$ content varies between 12.1 and 12.3, and $K_2O/Na_2O$ content ranges from 0.95 to 1.02. Furthermore, the granites in the study area belong to A-type granites with high silicon, low aluminium, and rich alkali formed in the late Yanshan period. They have a medium-grained granite structure and uniform lithology. Moreover, Laoshan granites are dominated by euhedral to semiautomorphic grain structures. The main minerals are quartz, potassium

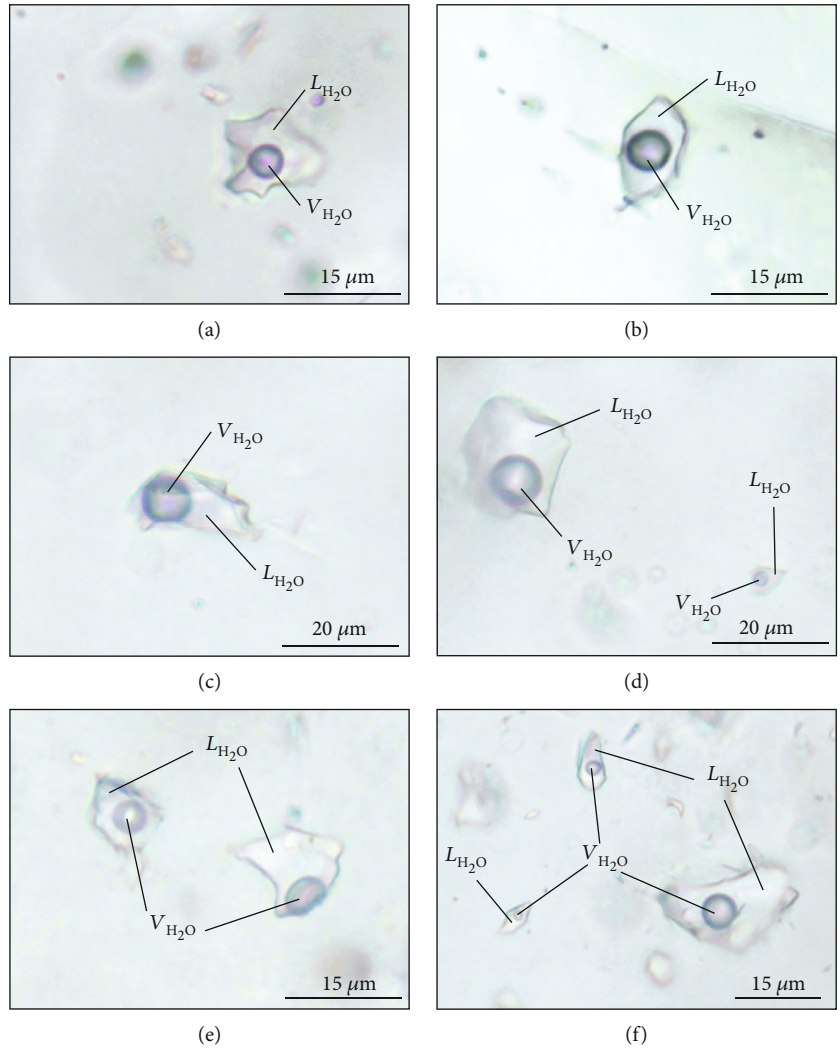


Figure 3: Gas-liquid two-phase fluid inclusions.

feldspar, and plagioclase, and the content of potassium feldspar is higher than that of plagioclase. The secondary mineral is predominately biotite, and the hornblende content is low.

*2.2. Samples.* Three samples from the Laojun cave, Ciguang cave, and the bedrock outside the cave were collected for fluid inclusion temperature measurements, salinity calibration, and H–O isotope testing. The target minerals tested were quartz. The samples were obtained from a section of the Laojun cave, Ciguang cave, innerwall rock of the Laojun cave, and innerwall rock of the Ciguang cave, all representing sections from intrusive plutons originating from the same period.

*2.3. Test Method.* Microscopic temperature measurements of the fluid inclusions were conducted at the Geological Fluid Laboratory of Jilin University, Changchun, China. H–O isotope measurements were performed by Beijing Zirconium Linghang Technology Co., Ltd, Beijing, China.

Petrographic sample analysis was conducted to establish the petrographic characteristics of the samples and select representative inclusion slices for further analysis. After the inclusion slices were pretreated, the temperature was measured using a Linkam THMS 600. Instrument calibration using the specified reference material showed an error of approximately ±2°C upon heating to 400°C and approximately ±0.1°C upon freezing to -22°C. The specific heating and cooling operations were in complete agreement with the experimental instruments and laboratory regulations [31].

The H–O isotopes were measured using a Thermo-Flash 253Plus isotope ratio mass spectrometer. For the determination of the hydrogen isotope, 10-20 mg of quartz single mineral samples ground through a 40–60 mesh was placed in a tin cup and dried in an oven at 90°C for 12 h to remove the adsorbed water on the mineral surface. After baking, the sample was placed in a high-temperature (1420°C) Thermo-Flash EA cracking furnace filled with glassy carbon particles. The water in the quartz inclusions was cracked and released at a high temperature and reacted with the glass carbon to generate CO and $H_2$. The generated CO and $H_2$ were then carried by high-purity helium (5 N) through the chromatographic column and entered the mass spectrometer

Table 1: Petrography characteristics of fluid inclusions.

| Position | Gas-liquid ratio (%) | Number | The long axis length ($\mu$m) | Number | Shape | Number |
|---|---|---|---|---|---|---|
| Ciguang cave | <3% | 8 | <3 $\mu$m | 36 | Quadrilateral | 201 |
| | 3%–5% | 79 | 3–6 $\mu$m | 166 | Irregular | 106 |
| | 5%–9% | 288 | 6–9 $\mu$m | 145 | Elliptical | 108 |
| | 9%–11% | 61 | 9–12 $\mu$m | 70 | Rectangular | 41 |
| | >11% | 29 | >12 $\mu$m | 48 | (Near) triangular | 9 |
| Laojun cave | <3% | 26 | <3 $\mu$m | 14 | Quadrilateral | 238 |
| | 3%–5% | 44 | 3–6 $\mu$m | 220 | Irregular | 88 |
| | 5%–9% | 278 | 6–9 $\mu$m | 150 | Elliptical | 126 |
| | 9%–11% | 95 | 9–12 $\mu$m | 76 | Rectangular | 24 |
| | >11% | 47 | >12 $\mu$m | 30 | (Near) triangular | 14 |
| Rock outside the cave | <3% | 13 | <3 $\mu$m | 12 | Quadrilateral | 210 |
| | 3%–5% | 95 | 3–6 $\mu$m | 128 | Irregular | 58 |
| | 5%–9% | 263 | 6–9 $\mu$m | 156 | Elliptical | 122 |
| | 9%–11% | 60 | 9–12 $\mu$m | 94 | Rectangular | 43 |
| | >11% | 23 | >12 $\mu$m | 64 | (Near) triangular | 21 |

Table 2: Microscopic temperature results of fluid inclusion.

| Sample | Type | Homogeneous phase | Homogenisation temperature (°C) | Freezing point temperature (°C) | Salinity (wt%) | Density (g/cm$^3$) | Number | Pressure (MPa) | Depth (km) |
|---|---|---|---|---|---|---|---|---|---|
| LJD-1 | $L+V$ | Liquid | 124.8–267.6 | -3.8–-1.5 | 2.56–6.14 | 0.80–0.98 | 17 | 28.61–37.99 | 2.86–3.80 |
| LJD-2 | | Liquid | 162.9–261.6 | -5.3–-2.3 | 3.85–8.27 | 0.83–0.95 | 10 | 31.99–43.56 | 3.20–4.36 |
| CGD-1 | | Liquid | 192.6–227.3 | -5.5–-2.0 | 3.37–8.54 | 0.87–0.92 | 10 | 30.74–44.27 | 3.07–4.43 |
| CGD-2 | | Liquid | 201.8–248.9 | -7.9–-1.8 | 3.05–11.59 | 0.84–0.95 | 15 | 29.89–52.28 | 2.99–5.23 |
| DW-1 | | Liquid | 162.5–230.8 | -4.1–-1.2 | 2.06–6.58 | 0.85–0.96 | 13 | 27.31–39.14 | 2.73–3.91 |
| DW-2 | | Liquid | 168.5–215.2 | -4.7–-1.7 | 2.89–7.44 | 0.87–0.96 | 13 | 29.47–41.38 | 2.95–4.14 |

Table 3: H–O isotopic composition of quartz and fluids in Laoshan granite.

| Sample | $\delta D_{V\text{-}SMOW}$ (‰) | $\delta^{18}O_{V\text{-}SMOW}$ (‰) | Isotopic equilibrium temperature (°C) | $\delta^{18}O_{H_2O}$ (‰) |
|---|---|---|---|---|
| Ciguang cave | -71.91 | 8.86 | 248.9 | -0.15 |
| Laojun cave | -83.58 | 8.82 | 261.6 | 0.39 |
| Host rock | -67.17 | 9.09 | 230.8 | -0.83 |

to determine the $H_2$ isotope ratio, $\delta$D. The test accuracy of this instrument for international standard materials exceeded 1‰ [32]. For oxygen isotope determination, 6 mg of quartz single mineral samples was ground through a 200 mesh and placed in the oven at 105°C for 12 h. The samples were then reacted with $BrF_5$ in a vacuum, and the oven temperature was increased to 580°C to extract oxygen from the minerals. A 5 Å molecular sieve sample tube was used to collect the extracted $O_2$. The instrument used in this experiment had a precision of ±0.2°C for the standard sample, and the relative standard used was V-SMOW [33].

## 3. Results and Discussion

*3.1. Fluid Inclusion Petrography.* The inclusions in the target pluton were well-developed. The quartz inclusions were predominately tested in this study. Two primary inclusion groups were identified: the first was fluid inclusions with a group, star, and isolated distribution in the middle part and a quartz growth zone, indicating primary inclusions (Figure 2). The second group predominately comprised inclusions grown along quartz fractures, with dense distributions and relatively small volumes. This study focused on the primary inclusions. Fluid inclusions in the following paragraphs refer to primary fluid inclusions.

At room temperature, the fluid inclusions showed various phase states and could be divided into two types according to their differences (Figure 3): gas-liquid two-phase fluid inclusions and pure liquid-phase fluid inclusions. Gas-liquid two-phase fluid inclusions represented the dominant type. Several fluid inclusions become pure liquid-phase inclusions after subsequent necking. The gas-liquid two-phase fluid

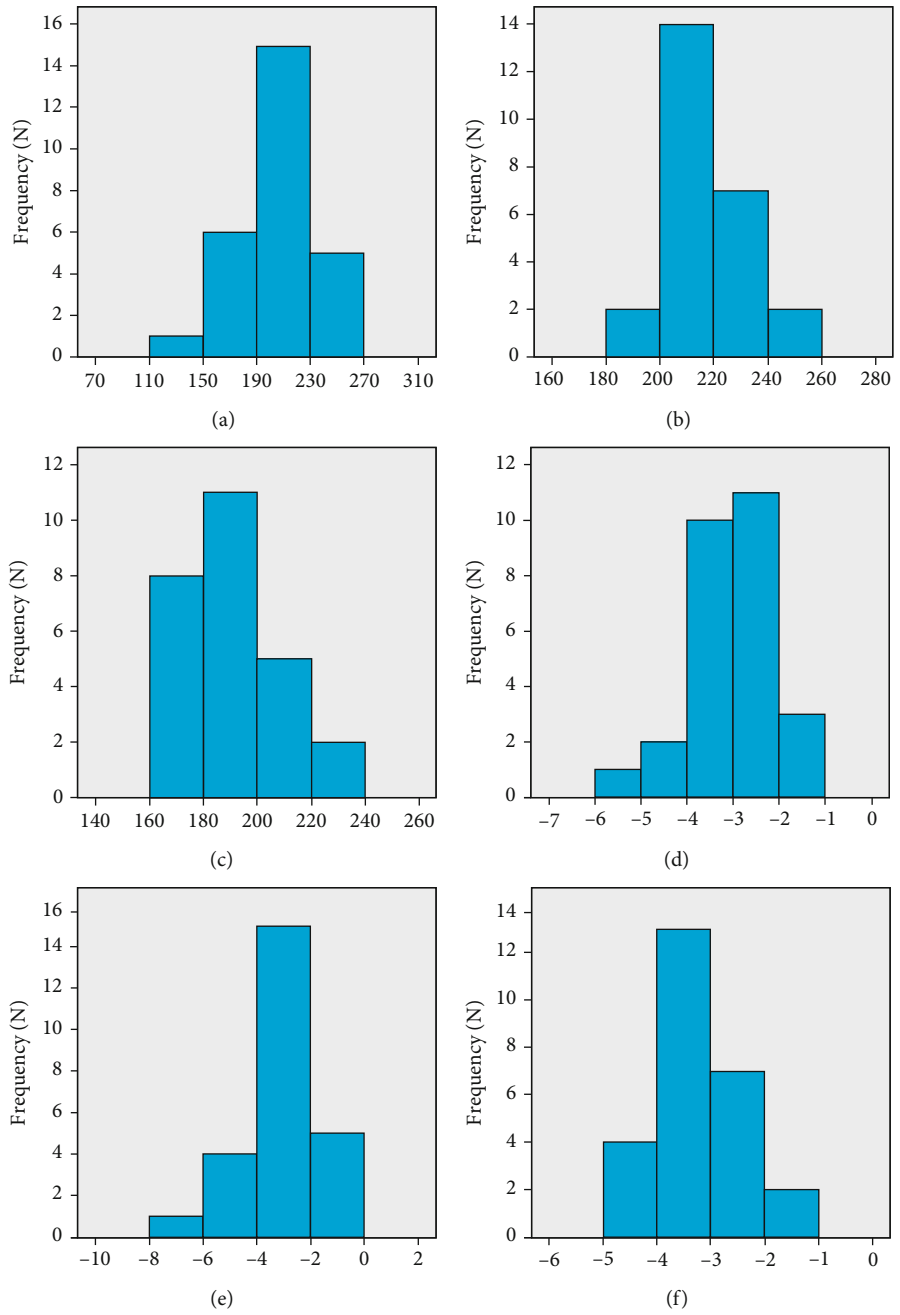


Figure 4: Continued.

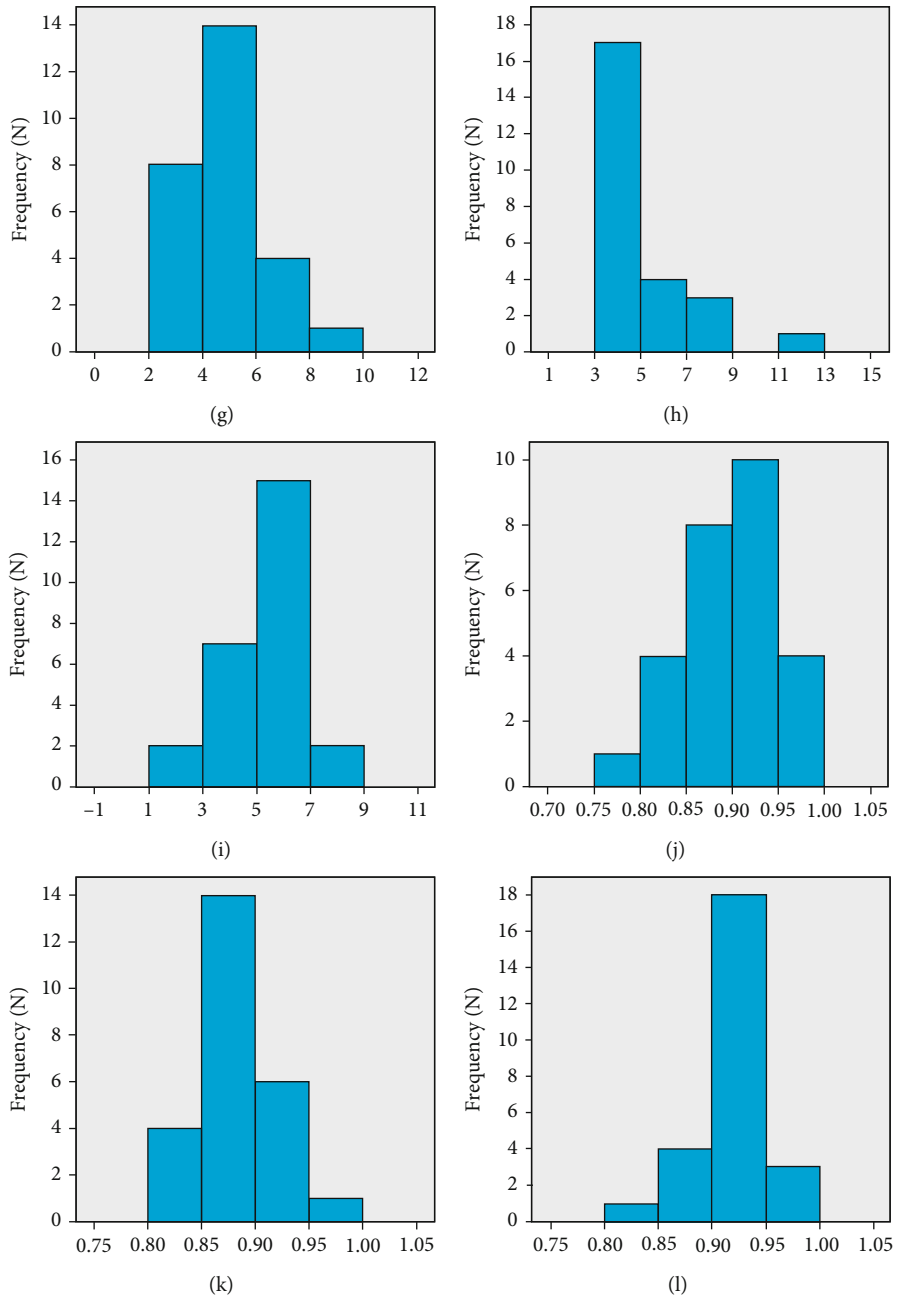


Figure 4: Histogram of temperature salinity and density at uniform temperature freezing point.

inclusions were predominately rich in liquid phase $L + V$ two-phase aqueous solution inclusions.

All the samples showed similar characteristics. The distribution characteristics of the samples' fluid inclusions were predominately group, star, strip, and isolated. The fluid inclusion shapes included irregular, rectangular, elliptical, quadrilateral, and (near) triangular. The long axis lengths ranged from 3 to 12 $\mu$m, and the gas-liquid ratio of the fluid inclusions was 3%–11%. The statistical results of the size and shape of the fluid inclusions are shown in Table 1.

*3.2. Temperature Measurement of Fluid Inclusions.* Temperature measurements were conducted on the rich liquid phase $L + V$ two-phase aqueous inclusions, with a total of 78 points tested. The test results are shown in Table 2. The microscopic temperature measurement data of the fluid inclusions show that the homogenisation temperature ranged between 162.5°C and 261.6°C and was mainly concentrated in the 160–240°C range. The distribution range of the freezing point temperatures was -7.9–1.2°C and predominately concentrated in the -5°C to -2°C range. The temperature of the fluid inclusions was medium-low. According to the temperature measurement results, the salinity of the inclusions ranged from 2.1 to 8.3 wt% and was mainly concentrated in the 2–7 wt% range. The density distribution range was 0.8–0.98 g/cm$^3$ and mainly concentrated in the 0.85–0.95 g/cm$^3$

range. Therefore, the fluid in the inclusions was characterised as a low-salinity and low-density fluid.

*3.3. H–O Isotope Test Results.* The results of the H–O isotope analysis are shown in Table 3. The analysis results show that the quartz $\delta D_{V\text{-}SMOW}$ value ranged from -83.58‰ to -67.17‰, and the $\delta^{18}O_{V\text{-}SMOW}$ value ranged from 8.82‰ to 9.09‰. According to Clayton et al. (1972), quartz $-\delta^{18}O_{H_2O}$ fractionation equation: $1000 \ln \alpha_{quartz-H_2O} = 3.38 \times 10^6 T^{-2} - 3.40$ ($T$ is the homogenisation temperature), the $\delta^{18}O_{H_2O}$ value of the quartz mineral fluid ranged between −0.83‰ and 0.39‰.

*3.4. Fluid Properties.* The primary fluid inclusions contained critical information such as temperature, pressure, salinity, density, and metallogenic depth of the fluid. The formula proposed by Hall et al. was used to calculate the salinity of the fluid inclusions in the $H_2O$–NaCl system using the freezing point drop temperature [34]:

$$W = 1.78 * T_m - 4.42 * 10^{-2} * T_{m^2} + 5.57 * 10^{-4} * T_m, \quad (1)$$

where $W$ is NaCl weight percentage (wt%$NaCl_{eq}$) and $T_m$ is the freezing point drop temperature (°C).

The salinity results are shown in Table 2. The salinity range of the fluid inclusions in the Laojun cave was 2.6–8.3 wt%, with an average value of 4.9 wt%. The salinity results were mainly concentrated in the 2–6 wt% range. In the Ciguang cave, the salinity ranged between 3.1 and 11.6 wt% and was mainly concentrated in the 3–5 wt% range. The average salinity value was 5 wt%. The salinity of the fluid inclusions in the rock samples outside the cave ranged from 2.1 to 7.4 wt%, with a 5.3 wt% average, and was concentrated in the 3–7 wt% range. The salinity frequency histogram is shown in Figure 4. Although the distribution range of the salinity values differed for each sample, the mean values and main concentration ranges were similar. Based on the salinity data for all the samples, the overall salinity of the fluid inclusions ranged from 2.1 to 8.3 wt% and was predominately concentrated in the 2–7 wt% range. Therefore, the fluid in the Laoshan granite fluid inclusions can be classified as a low-salinity fluid.

The fluid density was calculated using the formula proposed by Hass and Bodner for calculating the inclusion density of gas-liquid two-phase fluids in a NaCl-$H_2O$ system [35, 36]:

$$\rho = A + Bt + Ct^2, \quad (2)$$

where $\rho$ is the density of the NaCl solution (g/cm$^3$), $T$ is the uniform temperature (°C) of the fluid inclusion, and $A$, $B$, and $C$ are functions related to salinity $W$ (wt%):

$$\begin{aligned} A &= 0.993531 + 8.72147 \times 10^{-3} W - 2.43975 \times 10^{-5} W^2, \\ B &= 7.11652 \times 10^{-5} - 5.2208 \times 10^{-5} W + 1.26656 \times 10^{-6} W^2, \\ C &= -3.4497 \times 10^{-6} + 2.12124 \times 10^{-7} W - 4.52318 \times 10^{-9} W^2. \end{aligned} \quad (3)$$

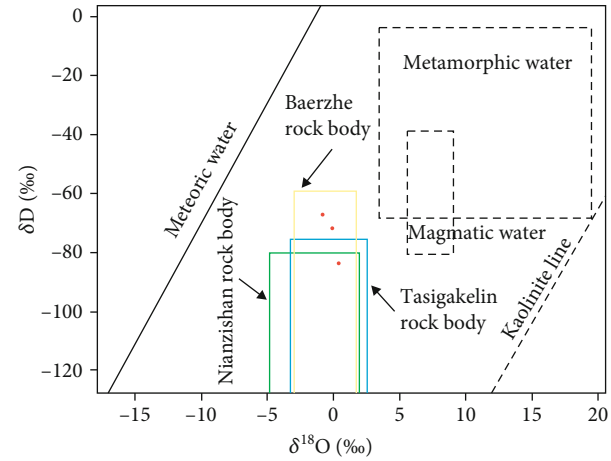


Figure 5: Relation diagram of Laoshan granite fluid $^{18}O_{H_2O}$ – $\delta D_{V\text{-}SMOW}$ (according to reference [44]).

The fluid density results are shown in Table 2. From all parts of the distribution of the fluid density value, three sections of the density distribution are the same, and the density of the concentrated scope was the same, ranging between 0.85 and 0.95 g/cm$^3$. The average fluid density within the two holes was similar. However, the fluid density of the hole was slightly greater than the average fluid density of the hole. Compared with the fluid density in other regions [37], the fluids in each part of the fluid inclusions in this study were classified as low-density fluids.

As only gas-liquid two-phase fluid inclusions were found in the Laoshan granite quartz samples, no $CO_2$-containing fluid inclusions were found to be symbiotic. Therefore, the formation pressure of the fluid inclusions could not be estimated using the isometric line intersection method in the $CO_2$–$H_2O$ system. When the fluid inclusion is in the gas-liquid NaCl–$H_2O$ system, it is difficult to determine the formation pressure of the fluid inclusion. However, the empirical formula proposed by Shao et al. (1998) can be used to obtain an estimate of the temperature at which deposits are formed [38–42], where a uniform temperature represents the lowest temperature of the fluid, that is, the lowest temperature of diagenesis. This empirical formula can be used for the pressure estimation of fluid inclusions in a NaCl–$H_2O$ system [43]:

$$\begin{aligned} T_0 &= 374 + 9.20 \times W, \\ P_0 &= 2190 + 262 \times W, \\ P_1 &= P_0 \times \frac{T_1}{T_0}, \end{aligned} \quad (4)$$

where $T_0$ is the initial temperature (°C), $W$ is the salinity (wt%$NaCl_{eq}$), $P_0$ is the initial pressure value (MPa), $P_1$ is the pressure value (MPa), and $T_1$ is the uniform temperature (°C).

In this study, we attempted to determine the mineral crystallisation temperature. Therefore, the initial temperature and pressure calculated by the formula were considered

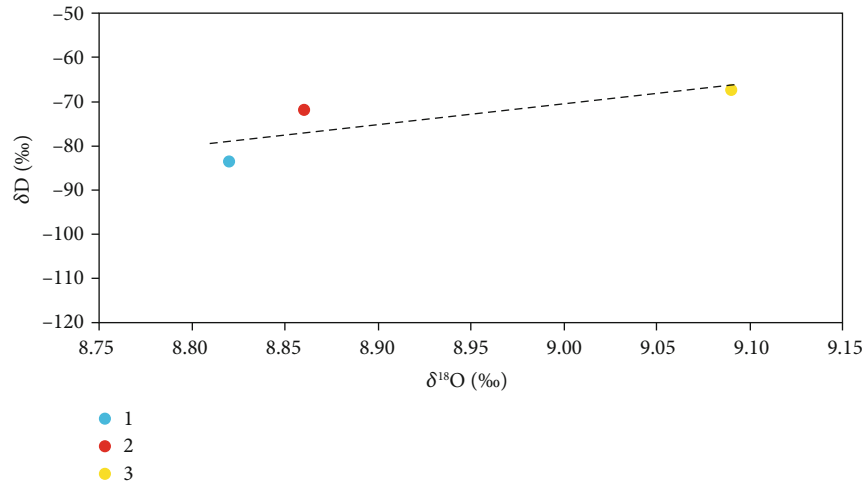


Figure 6: Correlation diagram of Laoshan granites $\delta^{18}O$-$\delta D$: 1: Laojun cave sample; 2: Ciguang cave sample; 3: bedrock sample.

the pressure and temperature of mineral crystallisation, and then, the pressure and depth of diagenesis were taken as the pressure and temperature, respectively.

The diagenetic pressure and emplacement depth of the Laoshan granite are shown in Table 2. The diagenetic pressure ranged from 27.31 MPa to 52.28 MPa (27.31–44.27 MPa after removing the abnormal values) and was mainly distributed in the 30–39 MPa range, with an average value of 34.93 MPa. The diagenetic depth ranged from 2.73 km to 5.23 km (2.73–4.43 km after removing abnormal values). The primary depth concentration range was 3.00–3.90 km, and the average value was 3.38 km.

*3.5. Fluid Source.* The fluid sources of the fluid inclusions with high salinities and low salinities vary. The former is generally affected by magmatic hydrothermal activity, whereas the latter may be affected by metamorphic hydrothermal activity and meteoric precipitation. The average salinity of the fluid inclusions in the Laoshan granite oval rock mass was 5.07 wt%, and the average density was 0.9 g/cm$^3$, indicating fluid with low salinity and density. Therefore, the diagenetic fluid may not be a single magmatic hydrothermal fluid.

The H–O isotopes in the quartz grains of the target rock mass were also studied, and the results obtained were used to define the source and evolution of fluids during diagenesis. In the hydrogen-oxygen isotope diagram of diagenetic fluid (Figure 5), it can be seen that all the sample points fall outside the region of metamorphic water and magmatic water and are tilted towards the meteoric line, indicating that the fluid inclusion is a mixture of magmatic water and meteoric water or groundwater related to meteoric water.

The solubility of water in granitic magma is closely related to pressure. When the pressure is lower than 200 MPa, the solubility of water decreases rapidly. When the magma pressure exceeds 200 MPa, the water content reached 7 wt%. For unsaturated magma, water saturation can only occur when the initial water content is 2 wt%, pressure is 50 MPa, and magma achieves a crystallisation degree of 30% [45, 46]. In this study, the pressure range calculated from the fluid inclusions ranged from 27.31 to 52.28 MPa. At this time, the solubility of water in the magma was lower than 2 wt%. Therefore, a large amount of water in the magma was separated out, and simultaneously, externally sourced meteoric water was not dissolved. The meteoric precipitation or groundwater mixed with magmatic water as the origin for the fluids is consistent with the previously calculated characteristics of low-salinity and low-density fluid inclusions.

*3.6. Formation Mechanism.* A study of the whole-rock H–O isotopes of granites in the Laoshan area by Yuan and Yu shows that rocks with strong degasification experienced delta after water-rock interaction. $\delta^{18}O$ and $\delta D$ were negatively correlated. However, after degassing from water-rock interactions, the $\delta^{18}O$ and $\delta D$ were positively correlated [47, 48], and the H–O isotope experimental data of this study showed a significant positive correlation (Figure 6). The positive correlation indicates that the Bashuihe pluton has experienced water-rock interactions without degasification.

Wang et al. and Wei et al. studied the rare earth elements and high field strength elements of Laoshan alkaline granites and found that there was strong hydrothermal activity in the late stage of magmatic activity and fluid enrichment occurred in the late stage of diagenesis [49, 50]. Wei et al. studied the H and O isotope geochemistry of the whole-rock and main rock-forming minerals of A-type granites in eastern China [51]. Their results revealed that the alkaline granites in Laoshan were affected by atmospheric precipitation exchange after the magmatic period. Wei et al.'s studies on zircon and whole-rock O isotopes, the Rb/Sr variation range, the distribution characteristics of $(^{87}Sr/^{86}Sr)_0$-1/Sr, and the variation law of $(^{87}Sr/^{86}Sr)_0$-$\delta^{18}O$ in the Laoshan pluton also established a significant hydrothermal exchange of meteoric water after the diagenetic magmatic stage [52].

H–O isotope experiments in this study and the results of previous studies indicate that the Bashuihe pluton in Laoshan is of great significance in the process of diagenesis. The hydrothermal activity was accompanied by intense hydrothermal activity, and the active hydrothermal fluid is formed by the mixing of magmatic water with external meteoric water or groundwater related to meteoric water. The

activity and source of hydrothermal fluid meet the requirements for the formation of larger primary caves in granite.

Primary cave formation in the Laoshan area occurred in the following manner: first, the magma temperature decreased substantially, and the magma fluid increased after the addition of meteoric water or groundwater. When the temperature of the magma decreased, the diagenetic mineral crystallisation rate accelerated, increasing the rate of magmatic diagenesis. An increase in magma fluid resulted in an increase in the activity of the fluid, enabling fluid migration and convergence. The accumulated fluid and volatilisation occupied more space, and the rapid condensation of magma sealed the accumulated fluid and volatiles in the rock mass, forming a large primary cave [53].

## 4. Conclusions

This study attempted to reconstruct the diagenetic evolution of granites in the Laoshan area using microthermometry, stable isotopes, and a whole-rock analysis. Our results revealed the following:

(1) The characteristics of the fluid in the Bashuihe pluton of the Laoshan granite are low temperature, low salinity, and low density. The average homogenisation temperature of the inclusions was 203.9°C, average salinity was 5.07 wt%, and average density was 0.9 g/cm$^3$. The diagenetic pressure estimated by the temperature measurement data of the fluid inclusions was concentrated in the 27.31–44.27 MPa range. The formation pressure of the pluton indicated a low-pressure environment, and the estimated emplaced depth was concentrated in the 3.00–3.90 km range, indicating a medium-shallow granitoid. The fluid in the diagenetic process has low salinity and low density, consistent with the conditions of primary cave formation in granites

(2) The analysis of H–O isotope data from the Bashuihe pluton indicates that the fluid moving in the diagenesis process was a mixture of magmatic water and meteoric water or groundwater related to meteoric water, which is consistent with previous research results

(3) The Bashuihe pluton formed under low-temperature and low-pressure conditions at a magma emplacement of approximately 3–3.9 km. The external fluid was added during the pluton formation process. The magma contained a significant number of volatiles and fluids, indicating rapid magma condensation during diagenesis. The volatiles and fluids formed an oval space in the condensed pluton, thereby forming an oval cave in the granite

(4) The discovery of oval caves in granite plutons provides a theoretical reference for the stability and safety of the development and utilisation of underground space and engineering buildings in granitic regions

## Data Availability

The data used to support the findings of this study are included within the article.

## Conflicts of Interest

The authors declare that they have no conflicts of interest.

## Acknowledgments

This work was financially supported by the opening foundation of the Key Laboratory of Marine Geology and Metallogeny, MNR, grant No. MGM202002; the Natural Science Foundation of Shandong Province, China (Grant No. ZR2020MD001); the National Natural Science Foundation of China (NSFC) (No. 41472155); and the Postgraduate Science and Technology Innovation Project of Shandong University of Science and Technology (SDKDYC190210).

## References

[1] J. Bruthans, M. Filippi, M. Slavik, and E. Svobodova, "Origin of honeycombs: testing the hydraulic and case hardening hypotheses," *Geomorphology*, vol. 303, pp. 68–83, 2018.

[2] J. R. Vidal-Romaní, M. Vaqueiro, and J. Sanjurjo, *Granite Landforms in Galicia*, Springer, Netherlands, 2014.

[3] H. W. Wellman and A. T. Wilson, "Salt weathering, a neglected geological erosive agent in coastal and arid environments," *Nature*, vol. 205, no. 4976, pp. 1097-1098, 1965.

[4] M. Arjunan and H. Achyuthan, "Tafoni along the east coast, Chennai to Mamallapuram, Tamil Nadu," *Current Science*, vol. 109, no. 1, pp. 195–201, 2015.

[5] N. S. Li, X. F. Shi, S. L. Zhao, and H. J. Yu, *Geology and Paleoglaciers of Mountain Laoshan, China*, Ocean Press, 2003.

[6] Z. A. Chen, "Some problem of granite geomorphological landscapes," *Geological Review*, vol. 53, no. S1, 2007.

[7] W. Wang, S. Z. Zhou, B. Y. Li, X. Bo, and X. Z. Feng, "Queries about the glacial potholes of Mountain Laoshan, China," *Quaternary Sciences*, vol. 31, no. 5, pp. 917–932, 2011.

[8] Z. J. Song, X. Q. Liu, Z. F. Gu et al., "Discussion on the granitic miarolitic caves and genesis of natural-mortars in the Mount Laoshan, China," *Quaternary Sciences*, vol. 32, no. 5, pp. 1046–1054, 2012.

[9] L. Guo, S. B. Xiang, and S. C. Zhao, *Laoshan in Glacial Period*, Shanghai Science and Technology Press, 2007.

[10] Z. Song, H. Liu, F. Meng et al., "Zircon U-Pb ages and Hf isotopes of Neoproterozoic meta-igneous rocks in the Liansandao area, northern Sulu Orogen, eastern China, and the tectonic implications," *Journal of Earth Science*, vol. 30, no. 6, pp. 1230–1242, 2019.

[11] G. T. Zhao, Q. C. Cao, D. Z. Wang, and H. M. Li, "Zirconicu U–Pb dating on the Laoshan granitoids and its significance," *Journal of Ocean University of Qingdao*, vol. 27, no. 3, 1997.

[12] G. T. Zhao, D. Z. Wang, and Q. C. Cao, "The geochemistry and genesis of the Laoshan granitoids, Shandong Province," *Geological Journal of China Universities*, vol. 3, no. 1, 1997.

[13] S. J. Wang, Y. S. Wan, W. Wang et al., "Forming ages of granites in Laoshan area of Shandong province—zircon SHRIMP U–Pb dating," *Shandong Land and Resources*, vol. 26, no. 10, 2010.

[14] Z. J. Song, W. J. Tang, X. Q. Liu et al., "Genesis and geological significance of granite caves in Laoshan of China," *Chemical Engineering Transactions*, vol. 46, pp. 763–768, 2015.

[15] G. T. Zhao and W. Z. Wang, "Compositional variation and its significance of amphiboles from Laoshan granitods," *Journal of Ocean University of Qingdao*, vol. 28, no. 4, pp. 98–103, 1998.

[16] Z. Su, J. C. Po, and J. D. Zhao, "Genesis of the potholes in China-comments on moulin discovery," *Geological Review*, vol. 63, no. 1, pp. 143–152, 2017.

[17] J. D. Zhao, J. Wang, and X. H. Yang, "Review, progress and prospect of the quaternary glaciations in eastern China ( east to 105°E)," *Journal of Glaciology and Geocryology*, vol. 41, no. 1, pp. 75–92, 2019.

[18] Y. Gao, Y. Niu, M. Duan et al., "The petrogenesis and tectonic significance of the early cretaceous intraplate granites in eastern China: the Laoshan granite as an example," *Lithos*, vol. 328-329, pp. 200–211, 2019.

[19] Z. J. Song, X. Y. Yuan, L. Gao, J. P. Li, X. Q. Liu, and W. J. Tang, "Quartz sand surface morphology of granitic tafoni at Laoshan, China," *Indian Journal of Geo-Marine Sciences*, vol. 48, no. 1, pp. 43–48, 2019.

[20] G. T. Zhao, D. Z. Wang, Q. C. Cao, and L. S. Yu, "Thermal evolution of I-A-type composite granite and its significance: the Laoshan granite as an example," *Science In China*, vol. 28, no. 4, pp. 296–302, 1998.

[21] Z. J. Song, X. Q. Liu, L. M. Gong, H. F. Li, Q. Chen, and Z. K. Gu, "Discovery of large bubble-like miarolitic granites in Laoshan and its significance," *Marine Geology Frontiers*, vol. 29, no. 12, pp. 1–5, 2013.

[22] Z. J. Song, H. M. Liu, X. Y. Yuan, H. B. Yan, Y. F. Sun, and H. N. Li, "A new genetic type of Tafoni: the mount Laoshan bubble-like cave granite as an example," *Acta Geologica Sinica*, vol. 93, Supplement 2, pp. 472-473, 2019.

[23] Z. Li, H. Liu, Z. Dun, L. Ren, and J. Fang, "Grouting effect on rock fracture using shear and seepage assessment," *Construction and Building Materials*, vol. 242, p. 118131, 2020.

[24] Z. Li, H. Zhou, D. Hu, and C. Zhang, "Yield criterion for rocklike geomaterials based on strain energy and CMP model," *International Journal of Geomechanics*, vol. 20, no. 3, p. 04020013, 2020.

[25] Z. Li, S. Liu, W. Ren, J. Fang, Q. Zhu, and Z. Dun, "Multiscale laboratory study and numerical analysis of water-weakening effect on shale," *Advances in Materials Science and Engineering*, vol. 2020, Article ID 5263431, 14 pages, 2020.

[26] Q. Meng, H. Wang, M. Cai, W. Xu, X. Zhuang, and T. Rabczuk, "Three-dimensional mesoscale computational modeling of soil-rock mixtures with concave particles," *Engineering Geology*, vol. 277, article 105802, 2020.

[27] C. Zhu, X. Xu, X. Wang et al., "Experimental investigation on nonlinear flow anisotropy behavior in fracture media," *Geofluids*, vol. 2019, Article ID 5874849, 9 pages, 2019.

[28] C. Zhu, M. He, M. Karakus, X. Cui, and Z. Tao, "Investigating toppling failure mechanism of anti-dip layered slope due to excavation by physical modelling," *Rock Mechanics and Rock Engineering*, vol. 53, no. 11, pp. 5029–5050, 2020.

[29] J. Z. Li and Z. J. Wan, "Lithodemic division and generation of com-posite batholith of the Laoshan granites," *Shandong Land and Resources*, vol. 10, no. 2, pp. 1–12, 1994.

[30] R. G. Liu, C. B. Wei, and Y. M. Yan, *Regional Geological Survey Report on The Lingshanwei Section I51C001001 1/250,000 of Qingdao Section J51C004001*, Shandong Institute of Geological Survey, 2004.

[31] R. J. Bakker, "Package FLUIDS 1. Computer programs for analysis of fluid inclusion data and for modelling bulk fluid properties," *Chemical Geology*, vol. 194, no. 1-3, pp. 3–23, 2003.

[32] B. Gong, Y.-F. Zheng, and R.-X. Chen, "An online method combining a thermal conversion elemental analyzer with isotope ratio mass spectrometry for the determination of hydrogen isotope composition and water concentration in geological samples," *Rapid Communications in Mass Spectrometry*, vol. 21, no. 8, pp. 1386–1392, 2007.

[33] "0184.13-1997 DT. Determination of oxygen isotopic composition in silicate and oxide minerals by bromine pentafluoride method," in *Standards for Geology and Mineral Industry of the People's Republic of China*, Ministry of Geology and Mines, PRC, 1997.

[34] D. L. Hall, S. M. Sterner, and R. J. Bodnar, "Freezing point depression of NaCl-KCl-H 2 O solutions," *Economic Geology*, vol. 83, no. 1, pp. 197–202, 1988.

[35] R. J. Bodnar, "A method of calculating fluid inclusion volumes based on vapor bubble diameters and P-V-T-X properties of inclusion fluids," *Economic Geology*, vol. 78, no. 3, pp. 535–542, 1983.

[36] J. L. Haas, "Physical properties of the coexisting phases and thermochemical properties of the $H_2O$ component in boiling NaCl solutions," *Bulletin of the United States Geological Survey*, vol. 1421, pp. 1–73, 1976.

[37] R. X. Li, S. H. Xu, Z. L. Yang, T. P. Liu, Y. Q. Wang, and T. C. Xie, "Geochemical study on fluid inclusion and H-O isotope of Daobeizhuangzi gold deposit in Xiadian Gold Field in Jiaodong Province," *Shandong Land and Resources*, vol. 33, no. 8, pp. 15–20, 2017.

[38] Z. M. He, *Study on Fluid Inclusions of the Zuoba Tungsten Deposit in Southern Jiangxi*, East China Institute of Technology, 2016.

[39] X. A. Liao, *The Research on Fluid Inclusions of the Zuoba Greisen Type Tungsten Deposit in Southern Jiangxi*, East China Institute of Technology, 2017.

[40] X. Wang, *Characteristics of Fluid Inclusions and Genesis of Changgou Gold Deposits in Hanyin County,Shanxi Province*, Chang'an University, 2017.

[41] M. L. Wei, *Study on the Characteristics and Significance of Fluid Inclusions in Yata Gold Deposit of Ceheng County, Guizhou Province*, Chengdu Univerisity of Technology, 2017.

[42] X. Y. Zhang, Y. Z. Hu, and X. Z. Liu, *Fluid Inclusions and H-O Isotopic Compositions in Weiruo Deposit of Lannigou Gold Deposit Area, Guizhou*, Bulletin of Geological Science and Technology, 2019.

[43] J. L. Shao, *Gold Ore Prospecting Mineralogy*, China University of Geosciences Press, Wuhan, China, 1988.

[44] H. P. Taylor, "The application of oxygen and hydrogen isotope studies to problems of hydrothermal alteration and ore deposition," *Economic Geology*, vol. 69, no. 6, pp. 843–883, 1974.

[45] H. L. Barnes, *Geochemistry of Hydrothermal Ore Deposits*, John Wiley & Sons, 1997.

[46] J. A. Whitney, *Ore Deposition Associated with Magmas*, Society of Economic Geologists, 1989.

[47] C. Yuan and J. S. Yu, "A study on the fossil hydrothermal convection system in the Qindao complex batholith of granitoids," *Geochimica*, vol. 23, no. 1, pp. 50–59, 1994.

[48] X. Wang, B. Li, S. J. Guan, O. Nadeau, and G. Tang, "Mineralized granitic porphyry of the Yangla copper deposit, Western Yunnan, China: geochemistry of fluid inclusions and H-O, S, and Pb isotopes," *Geofluids*, vol. 2020, Article ID 4391703, 32 pages, 2020.

[49] R. Wang, G. Zhao, D. Wang, J. Lu, and S. Xu, "Differentiation and accumulation of fluids in A-type granites: evidence from accessory mineral study," *Chinese Science Bulletin*, vol. 45, no. 17, pp. 1609–1613, 2000.

[50] C. S. Wei, Y. F. Zheng, and Z. F. Zhao, "Zircons rich in thorium in alkaline A-type granite: mineralogical studies and petrological implications,," *Chinese Science Bulletin*, vol. 50, no. 10, pp. 1016–1023, 2015.

[51] C. S. Wei, Y. F. Zheng, and Z. F. Zhao, "Hydrogen and oxygen isotope geochemistry of A-type granites in the continental margins of eastern China," *Tectonophysics*, vol. 328, no. 1-2, pp. 205–227, 2000.

[52] C. S. Wei, Y. F. Zheng, and Z. F. Zhao, "Nd-Sr-O isotopic geochemistry constraints on the age and origin of the A-type granites in eastern China," *Acta Petrologica Sinica*, vol. 17, no. 1, pp. 95–111, 2001.

[53] W. Zhao, Z. Guo, M. Lei et al., "Volcanogenic $CO_2$ degassing in the Songliao continental rift system, NE China," *Geofluids*, vol. 2019, Article ID 8053579, 14 pages, 2019.